

Cite this: DOI: 10.1039/c2dt30343d

www.rsc.org/dalton

PAPER

Self-assembled NiO–ZrO₂ nanocrystals with mesoscopic void space: An efficient and green catalyst for C–S cross-coupling reaction in water†

Nabanita Pal and Asim Bhaumik*

Received 15th February 2012, Accepted 12th April 2012

DOI: 10.1039/c2dt30343d

New NiO–ZrO₂ nanocrystals (MNZ-1) with mesoscopic self-assembly have been synthesized by using a non-ionic surfactant as the structure directing agent (SDA) *via* evaporation induced self-assembly (EISA) method. Powder X-ray diffraction (PXRD), N₂ sorption study and transmission electron microscopic (TEM) image analyses revealed the cubic structure, mesoporosity and mesoscopic self-assembly of *ca.* 7.0 nm sized tiny nanocrystals in the material. MNZ-1 catalyzes the aerobic aryl–sulfur cross-coupling reactions for a series of aryl-iodides with 4-chlorothiophenol in environment friendly water medium at elevated as well as room temperature. Pure ZrO₂ mesoporous nanocrystals are inactive, whereas pure NiO nanocrystals showed much lower catalytic activity under similar reaction conditions. The MNZ-1 nanocatalyst is completely non-air sensitive, inexpensive and effective for the synthesis of a series of essential biomolecules derived from diaryl sulfides.

Introduction

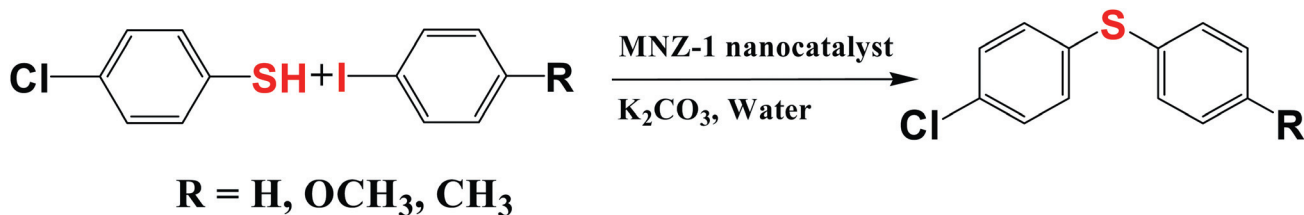
In recent decades, self-aggregation of nanoparticles to form nanostructures of different dimensions has drawn wide-scale attention among researchers of various disciplines.¹ Weak non-covalent intermolecular forces like van der Waals forces,² hydrogen bonding interaction,³ host–guest interaction⁴ *etc.* are responsible for the formation of self-assembled nanostructures. Their advanced applications in a number of pioneering research areas like optics, microelectronics, nanodevices, magnetism, catalysis and biological science are explored.⁵ Moreover, due to their large surface to volume ratio some exceptional properties like quantum effect, macroscopic quantum tunnel effect *etc.* are observed in those self-assembled nanoparticles (having particle size below 10 nm), which are absent in their corresponding bulk materials.⁶ There are numerous chemical methods like hydrothermal,⁷ evaporation induced self-assembly (EISA),⁸ microwave assisted heating,⁹ microemulsion *etc.* which are known for the fabrication of various nanoparticles of metal, metal oxides, metal sulfides, selenides and chalcogenides *etc.* with uniform size.¹⁰ But comparatively less attention has been paid to the self-assembled mixed oxide nanoparticles¹¹ having sizes less than 10 nm and specially their use in eco-friendly catalytic reactions. Organized superstructures of the mixed oxide nanoparticles may play a key role in the field of catalysis technology.

It is pertinent to mention that since the oxide based nanocrystals self-assemble to form mesoporous material in the presence of block copolymer surfactants, the removal of the template molecules from the solid composite materials could generate mesoscopic void spaces. Thus, the porosity and surface area generated through this process can play a very crucial role in the gas storage, ion-adsorption, ion-exchange, biomolecule separation, catalysis, drug delivery *etc.*¹² To date reports on the self-aggregated oxide nanoparticles into crystalline mesoporous framework are limited to TiO₂,^{5e} CeO₂,¹³ ZrO₂,¹⁴ SnO₂,¹⁵ SrTiO₃,¹⁶ WZrO₂,¹⁷ *etc.* Gawande *et al.* has recently reported the synthesis of MgO–ZrO₂ nanoparticles through ultra-dilution method, which produces a tetragonal zirconia phase.¹⁸ Hence, the synthesis of mixed metal oxide nanoparticles containing cubic ZrO₂ as an integral part of the superstructure and their self-assembly is very challenging and highly desirable.

Diaryl sulfides formed *via* C–S cross-coupling reaction from aryl halides bearing different nucleophilic phenyl rings have significant roles in biological, pharmaceutical, and material research.¹⁹ Transition metals like Fe, Ni, Pd, Cu, Co based salts mediated C–S coupling reactions in various organic solvents and an inert atmosphere offer a homogeneous media for those catalytic reactions. But these reactions suffer from the disadvantage of catalyst separation, environmental hazards, *etc.*²⁰ Moreover, formation of diaryl disulfides as a byproduct due to additional S–S bond formation decreases the yield of the desired product as well as makes the reaction more difficult. Very recently we have developed Cu-grafted functionalized mesoporous catalyst, which can be successfully employed for a series of facile C–S cross-coupling reactions in different polar organic solvents.²¹ Ranu *et al.* has reported a microwave-assisted Cu nanoparticle catalyzed aryl–sulfur coupling reaction in less than

Department of Materials Science, Indian Association for the Cultivation of Science, Jadavpur, Kolkata–700 032, India.
E-mail: msab@iacs.res.in

†Electronic supplementary information (ESI) available. See DOI: 10.1039/c2dt30343d



Scheme 1 General scheme for C–S cross coupling reaction.

10 min.²² But the reaction was conducted at relatively higher temperature and in organic solvent DMF. Different Ni complexes applied for this coupling reaction by various research groups, showed better activity in hazardous organic solvents and homogeneous medium.²³ To the best of our knowledge, there is no report on the aryl–sulfur coupling reactions using heterogeneous Ni based nanocatalyst and in completely non-polluting water as reaction medium.

In this report, we describe the synthesis of self-assembled NiO–ZrO₂ nanoparticles having cubic structure *via* an EISA method using a non-ionic Pluronic F127 template and citric acid (CA). CA helps the ordered assembling of the nanoparticles to form mesoscale structures by minimizing the hydrolysis and condensation rate of the metal precursors.²⁴ The highly crystalline stable nanomaterials thus formed showed good catalytic activity in the coupling of iodoaryl compounds with thiol compounds at moderately elevated temperature in aqueous media containing mild base, K₂CO₃ (Scheme 1). The aerobic synthesis on this mixed oxide nanoparticles and easy catalytic reactions reported herein is completely green and thus environment friendly.

Experimental section

Synthesis of MNZ-1 nanoparticles

We have prepared the mixed oxide nanomaterial MNZ-1 using non-ionic block copolymer Pluronic F127 ($M_{av} = 12\,600$, EO₁₀₆PO₇₀EO₁₀₆, Sigma-Aldrich) as structure directing agent (SDA), 35 wt% hydrochloric acid (HCl, E-Merck) to maintain the acidity of the medium, citric acid (CA, Loba Chemie), nickel(II) nitrate Ni(NO₃)₂ (Loba Chemie) as the source of nickel and zirconium(IV) butoxide [Zr(OC₄H₉)₄, Sigma-Aldrich] as the source of zirconium. In a typical synthesis of this self-assembled nanoparticle, 1.65 g HCl was added and stirred well in 20 mL absolute ethanol. Then, 1 g Pluronic F127 template was added to the acidic solution and allowed to stir for 10–15 min until dissolution. This is followed by the addition of 0.63 g of CA with vigorous stirring for about 1.5 to 2 h at room temperature (RT). Then, 2.95 g (10 mmol) Ni(NO₃)₂ was added to the mixture and after dissolution 3.85 g (10 mmol) Zr(OC₄H₉)₄ was put dropwise in the green solution. The resulting mixture was kept on stirring covering with PE film for overnight and finally aged without stirring at RT for solvent evaporation during 2 to 3 days (depending on the concentrations) to get solid green powder. Calcination was carried out at 773 K for 5–6 h in the presence of air to obtain a deep green template free mesoporous NiO–ZrO₂ (named MNZ-1).

General procedure for aryl–sulfur coupling reaction over cubic MNZ-1 nanoparticles

A mixture of iodoaryl compound (Sigma-Aldrich, 1.0 mmol) and 4-chlorothiophenol (Sigma-Aldrich, 1.2 mmol) in 3 mL of water was taken in a round-bottomed flask, K₂CO₃ (E-Merck, 280 mg, 2.0 mmol) and 50 mg catalyst were added in the mixture. The mixture was then heated at 353 K in a temperature controlled oil bath fitted with a water condenser and the progress of the reaction was monitored by TLC. After completion of the reaction, the reaction mixture was allowed to cool and the catalyst was separated by simple filtration. The catalyst was then washed and the filtrate was extracted with Et₂O. The combined organic layer was repeatedly washed with water followed by 10% aqueous NaOH and brine solution. Then the organic layer was dried over anhydrous Na₂SO₄ (E-Merck) and evaporated to dryness to give the crude product diphenylsulfide derivatives as a solid product. The product was further dissolved in *n*-hexane and purely crystalline product was separated from that mixture. The isolated crude product was characterized by ¹H, ¹³C NMR and FT IR analysis, respectively. The general scheme for aryl–sulfur cross coupling reaction over MNZ nanoparticles is shown in Scheme 1.

Characterizations

The small and wide angle powder X-ray diffraction (XRD) patterns of the MNZ-1 material were recorded on a Bruker AXS D-8 Advance diffractometer operated at 40 kV voltage and 40 mA current and calibrated with a standard silicon sample, using Ni-filtered Cu K_α ($\lambda = 0.15406$ nm) radiation. Nitrogen adsorption–desorption isotherms were achieved using a Beckman Coulter SA 3100 surface area analyzer at a temperature of 77 K. Prior to this analysis the sample was degassed at 423 K. For recording TEM (transmission electron microscopy) and HR TEM (high resolution transmission electron microscopy) images a JEOL JEM 2010 transmission electron microscope was used. JEOL JEM 6700F field emission scanning electron microscope (FE SEM) with an energy dispersive X-ray spectroscopic (EDS) attachment was used to analyze the morphology of the sample and its surface chemical composition. UV-visible diffuse reflectance spectrum was recorded using a Shimadzu UV 2401PC spectrophotometer with an integrating sphere attachment and using BaSO₄ pellet as background standard. ¹H and ¹³C NMR experiments were carried out on a Bruker DPX-300 NMR spectrometer. Fourier transform infrared (FT IR) spectrum was recorded on KBr pellets by using a Nicolet MAGNA-FT IR 750 spectrometer Series-II. The Ni content in the sample was

measured using Shimadzu AA-6300 atomic absorption spectrophotometer (AAS) using the aqueous solution of the sample digested in a minimum quantity of HF/HNO₃.

Results and discussions

Powder XRD analysis

The small powder X-ray diffraction pattern of the calcined MNZ-1 sample is shown in Fig. 1. One relatively stronger peak near $2\theta = 0.75^\circ$ indicates the distribution maximum of the distance of two nearest particle centers. The peak corresponds to the inter-nanoparticle separation *i.e.* the distance of particle center to particle center of *ca.* 12.61 nm (Table 1). The wide angle XRD pattern of the highly crystalline MNZ-1 sample depicted in Fig. 2b exhibits well-resolved highly intense peaks characteristics of the cubic phase of ZrO₂ nanoparticles along with highly aligned cubic phase of NiO. Peaks at $2\theta = 30.3^\circ$, 35.14° , 50.48° and 60.2° reveal the presence of (111), (200), (220) and (311) planes, respectively of cubic ZrO₂ according to JCPDS CAS number 27-0997; with a lattice parameter of 0.509 nm.²⁵ On the other hand, diffraction peaks at $2\theta = 37.28^\circ$, 43.28° , 62.9° and 75.44° as well as their relative intensities correspond well with the (111), (200), (220) and (311) crystal planes of face-centered cubic NiO (JCPDS No. 04-0835), respectively with a lattice parameter 0.418 nm.²⁶ The diffraction peaks of MNZ-1 sample has been compared with the powder XRD patterns of pure NiO and ZrO₂. There is no impurity of any other phases of both the oxides. Presence of this type of mixed phase for multimetal oxide nanoparticles is particularly important in catalytic reactions.¹⁸

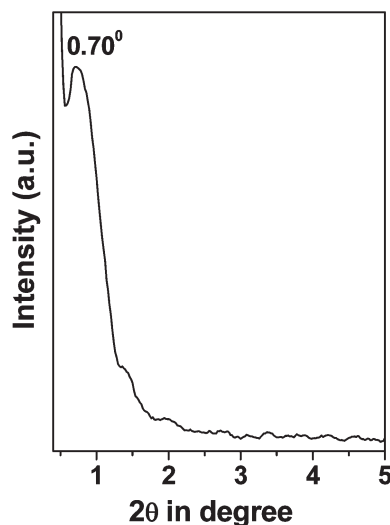


Fig. 1 Small angle XRD pattern of the MNZ-1 sample.

N₂ sorption study

Nitrogen adsorption–desorption isotherms of the self-assembled NiO–ZrO₂ is shown in Fig. 3. Brunauer–Emmett–Teller (BET) surface area, average pore diameter, and pore volume of the material estimated from sorption study are exhibited in Table 1. The sorption isotherms are of type IV pattern, characteristic of typical mesoporous materials.²⁷ The prominent desorption hysteresis at higher P/P_0 indicates capillary condensation within the

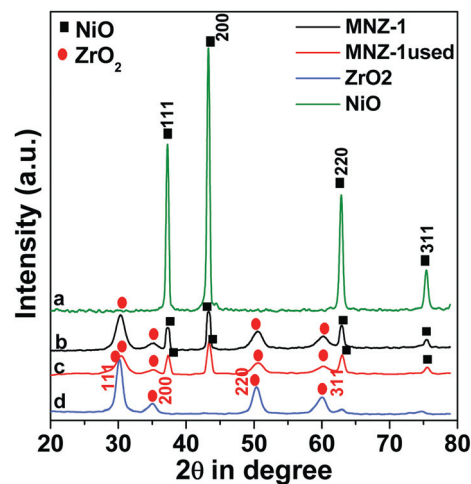


Fig. 2 Wide angle XRD pattern of (a) pure NiO, (b) MNZ-1, (c) MNZ-1 used (after the catalytic reaction) and (d) pure ZrO₂ samples.

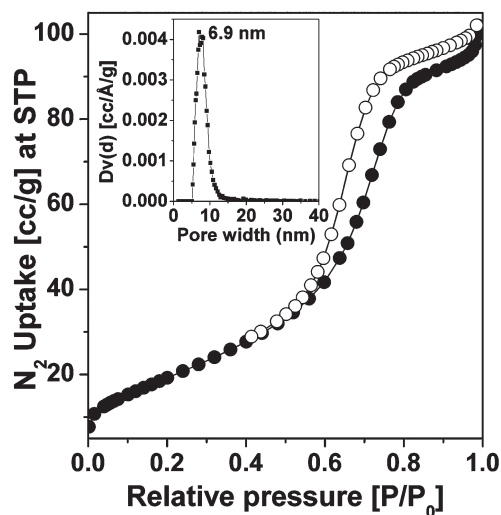


Fig. 3 N₂ adsorption (●)–desorption (○) isotherms of MNZ-1 measured at 77 K. The corresponding pore size distribution is shown in the inset.

Table 1 Physicochemical data of the mesoporous material MNZ-1

Ni : Zr synthesis gel	Ni : Zr product (EDS)	<i>d</i> spacing from XRD (nm)	BET surface area (m ² g ⁻¹)	Pore volume (cc g ⁻¹)	Pore width (nm)	Average particle size (nm)	Ni percentage (AAS)
1 : 1	1.15 : 1	12.61	77.00	0.15	6.90	5.71	9.13

large mesopores.²⁸ Pore size distribution plot shown in the inset of Fig. 3 obtained by applying the NLDFT (non-local density functional theory) method²⁹ gives a sharp peak with an average pore width value of 6.9 nm, which could be attributed to the interparticle mesoporosity. Thus the average

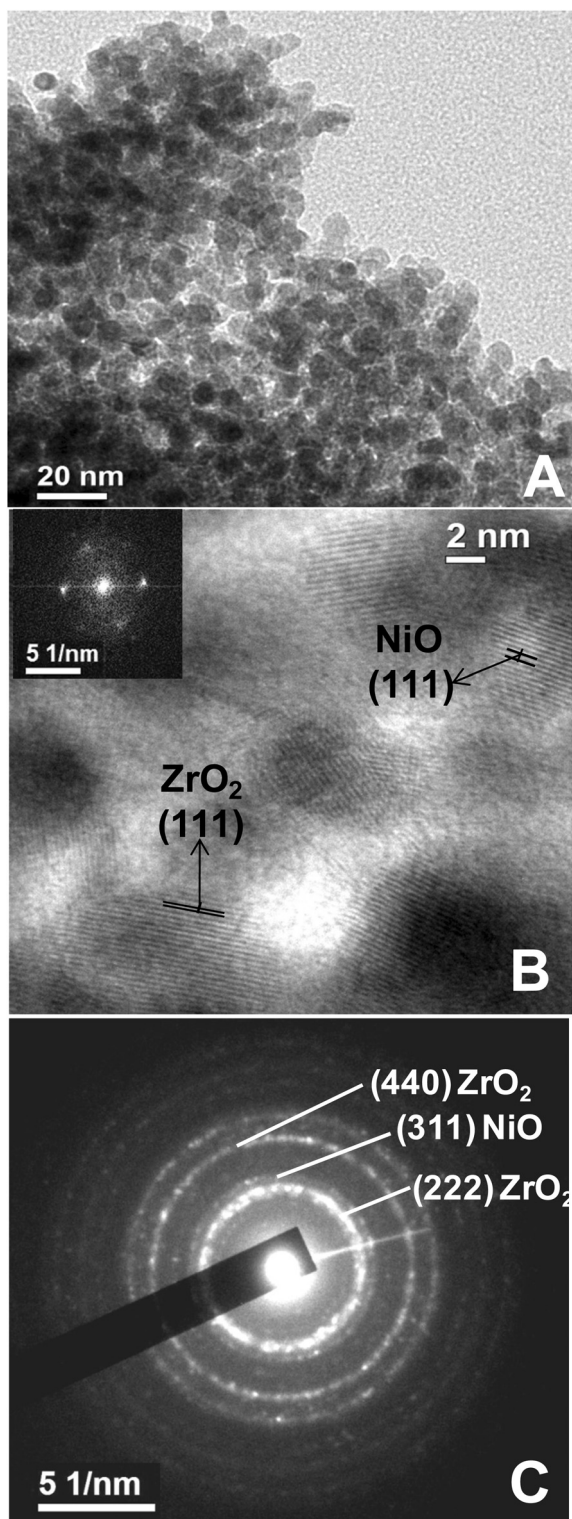


Fig. 4 A: TEM image of aggregated MNZ-1 nanoparticles. B: HRTEM image of the sample with FFT pattern in inset. C: SAED pattern of MNZ-1.

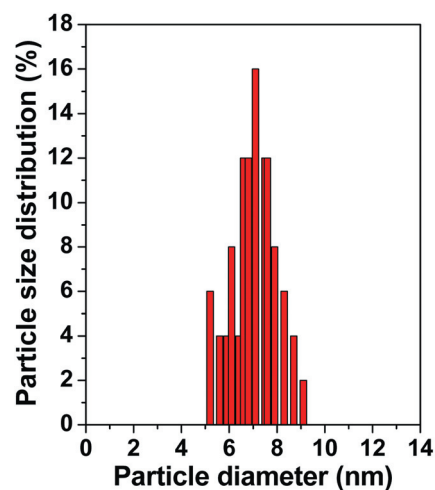


Fig. 5 Particle size distribution plot of MNZ-1 obtained from TEM image.

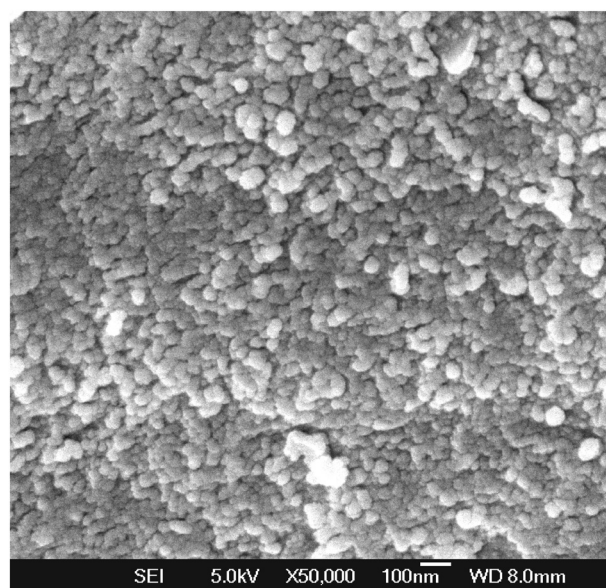


Fig. 6 FE SEM image of MNZ-1 nanoparticles.

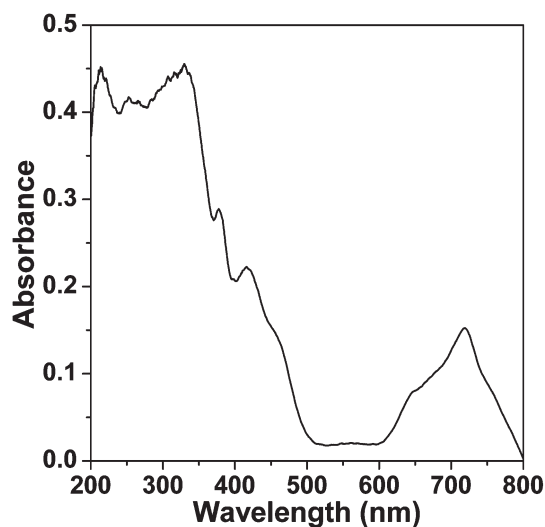


Fig. 7 UV-visible diffuse reflectance spectrum of the mesoporous mixed oxide MNZ-1.

Table 2 C–S coupling reaction over MNZ-1 sample

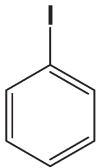
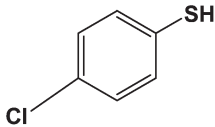
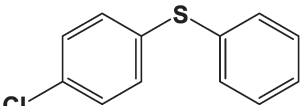
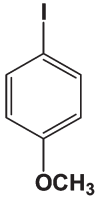
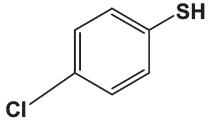
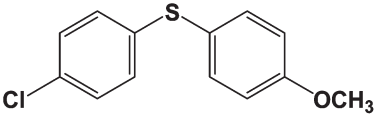
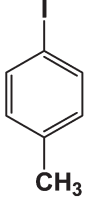
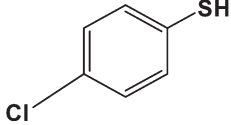
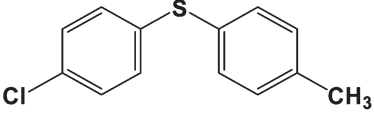
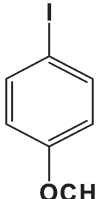
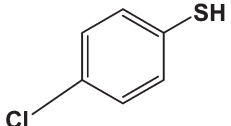
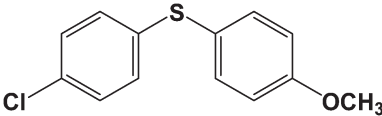
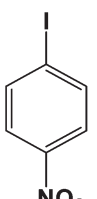
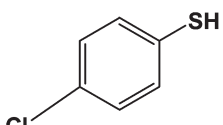
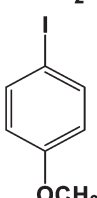
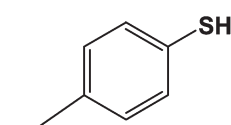
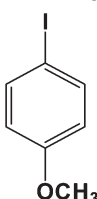
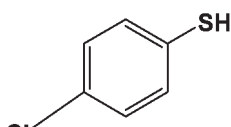
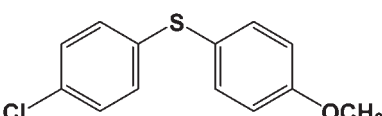
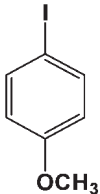
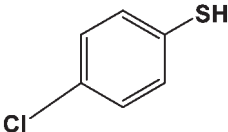
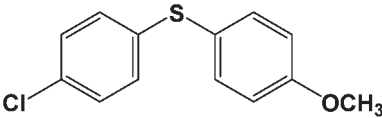
Entry	Aryl Iodide	Thiol	Product	Yield (%)
1				62.0
2				89.0
3				68.0
4 ^a				39.0
5			—	—
6 ^b			—	—
7 ^c				15.6

Table 2 (Contd.)

Entry	Aryl Iodide	Thiol	Product	Yield (%)
8 ^d				36.4

Reaction conditions: aryl iodide = 1 mmol, thio compound = 1.2 mmol, solvent: water = 3 ml, K_2CO_3 = 2 mmol, catalyst = 0.05 g, time = 24 h.^a Reaction was carried out at room temperature for 36 h. ^b Reaction was carried out in the absence of any catalyst. ^c NiO material alone (in absence of ZrO_2 support) was used as catalyst. ^d Reaction was carried out with 1 : 1 (wt) mixture of pure NiO and ZrO_2 .

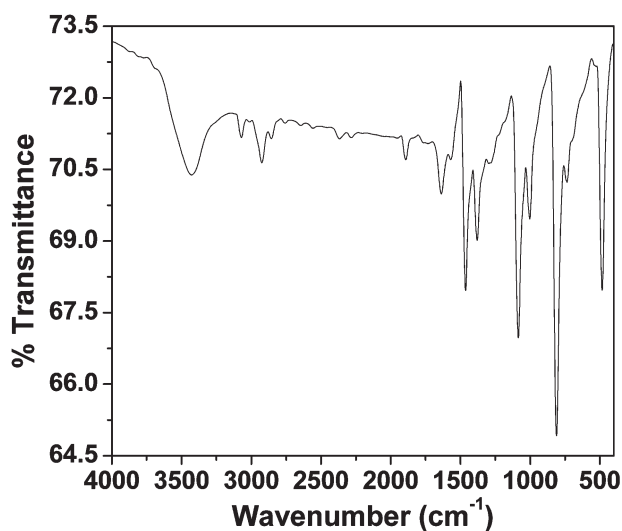


Fig. 8 FT IR spectrum of the isolated C–S coupling product (Table 2, entry 2).

particle size obtained by subtracting this pore width value from the value of inter-nanoparticle separation (from PXRD) is *ca.* 5.71 nm.

Electron microscopic analyses

The transmission electron microscopy (TEM) image of the aggregated nanoparticle is displayed in Fig. 4A. From this image it is evident that the average particle size of MNZ-1 is *ca.* 5–8 nm with an interparticle porosity (low electron density spots) of *ca.* 5–6 nm. Thus the size of the particle resembles well with the data obtained from the N_2 sorption study. The nanocrystalline feature of the pore walls of the tiny self-assembled MNZ-1 nanoparticles is clear from the representative HR TEM image of the sample shown in Fig. 4B. The well-resolved crystal lattice fringes agree well with the *d* spacing value of both NiO and ZrO_2 oxides. The FFT pattern in the inset confirms the cubic nature of the highly crystalline mixed oxide. Further, this HR TEM image (Fig. 4B) suggested intergrowth of the nanocrystals with very strong surface interactions between nickel oxide and zirconia. Although, the solubility of Ni^{2+} ions

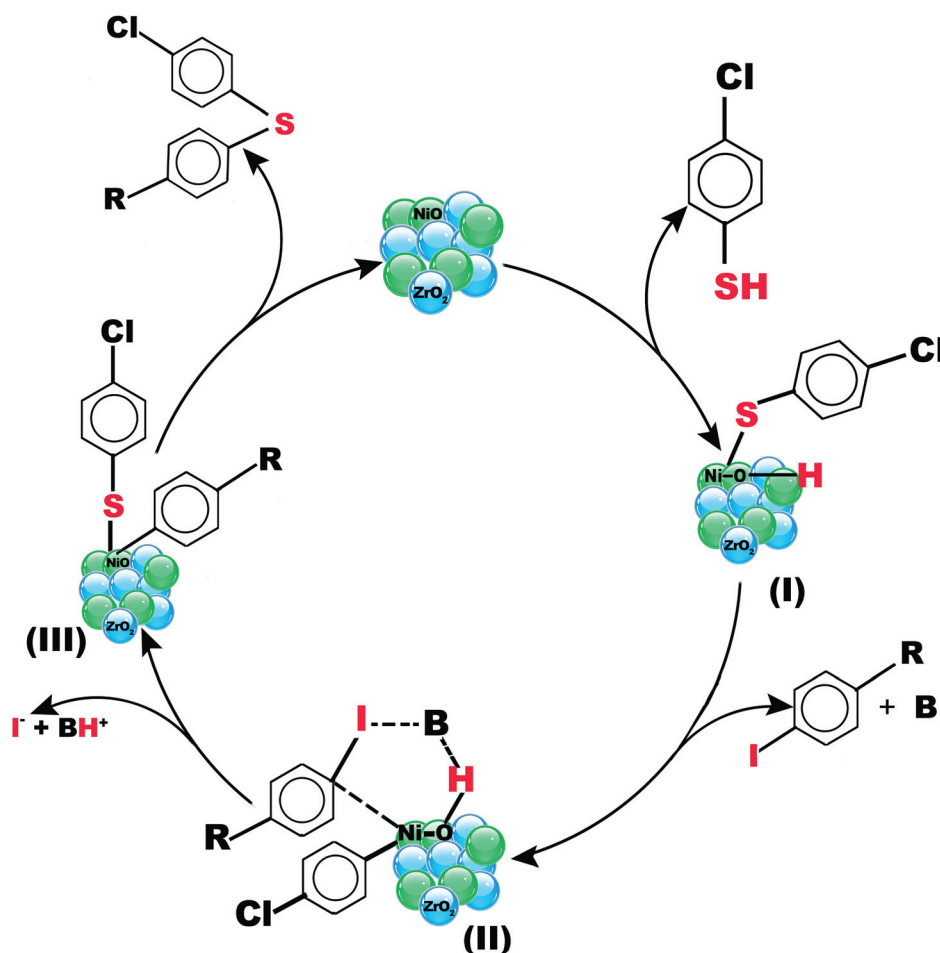
in the ZrO_2 lattice is quite low,³⁰ this strong surface interaction could stabilize the cubic ZrO_2 phase in the MNZ-1 nanocrystal. Selected area electron diffraction pattern (SAED) of the sample depicted in Fig. 4C shows a number of diffraction rings of several planes, which resemble well the *d*-spacings of the cubic nickel and zirconium oxide phases as obtained from PXRD. The particle distribution plot obtained from the TEM analysis shows a maximum *ca.* 7.00 nm signifying that the average size of most of the particles is 7.0 nm (Fig. 5). The textural property investigated by the FE SEM image (Fig. 6) indicates that small spherical particles are aggregated throughout the specimen. The uniform spherical texture of the nanocrystals and their self-assembly is similar to that observed in TEM analysis. The EDS analysis data (Table 1) reveals the atomic percentage ratio of Ni and Zr in the calcined product is 1.15 : 1, which is similar to the molar ratio of those in the synthetic gel.

UV-visible spectroscopic study

The UV-visible diffuse reflectance spectrum of NiO– ZrO_2 mixed oxide nanoparticles is shown in Fig. 7. Strong absorbance maxima near 218 nm could be attributed to the oxygen to metal charge transfer transition of octahedral Zr(IV) in ZrO_2 .³¹ Whereas no peak for d–d transition is seen there since Zr(IV) has electronic configuration d^0 . On the contrary, the UV band near 247 nm could be assigned to the $O \rightarrow Ni^{2+}$ charge transfer transition in the NiO phase. In addition to that the presence of d–d transition bands of octahedrally coordinated Ni(II) are evident from peaks near 415, 643 and 718 nm.³² Thus the UV-visible diffuse reflectance spectrum of MNZ-1 suggested the presence of ZrO_2 and NiO phases.

Catalytic activity of MNZ-1 in C–S coupling reaction

Here, we have explored the catalytic efficiency of the NiO– ZrO_2 mixed oxide nanoparticles in C–S cross-coupling reactions of different iodoaryl substrates with the thio compound 4-chlorothiophenol in green solvent water using K_2CO_3 as a mild base. Different diarylsulfides obtained with moderately high yield ranging from 62% to 89% are summarized in Table 2.³³ Almost no product formation was observed in case of strongly deactivated aromatic substrate containing $-NO_2$ substituent. It is



Scheme 2

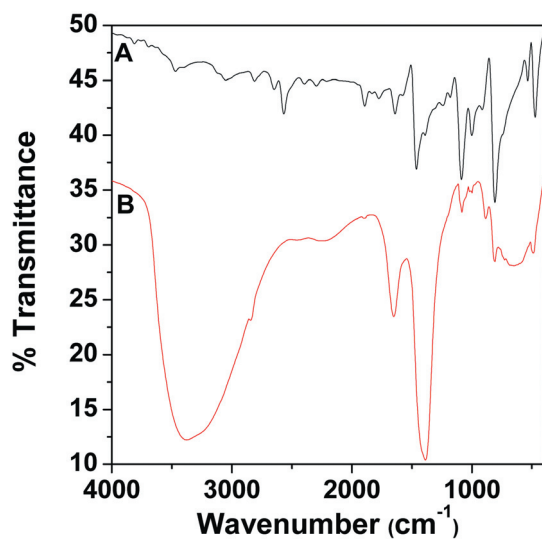


Fig. 9 FT IR spectra of A: 4-chlorothiophenol and B: MNZ-1 catalyst isolated during the reaction.

further evident that under similar reaction conditions the product yield is higher in case of those iodobenzenes containing electron donating groups (OCH_3/CH_3), which have a more activated

benzene ring *i.e.* the formation of coupled product increases with the increasing electron donating ability of the substituent in the iodobenzene ring. The FT IR spectrum of the isolated crude product (of entry 2) shown in Fig. 8 reveals that there is no stretching vibration band for the S–S bond near $500\text{--}540\text{ cm}^{-1}$, which indicates very little possibility of diaryl disulfide formation. Moreover, the absence of the stretching frequency of the S–H bond near $2550\text{--}2600\text{ cm}^{-1}$ proves the splitting of this bond together with the formation of a C–S bond. The reaction was carried out both at room temperature (Table 2, entry 4) as well as at elevated temperature. Although, the yield is lower at low temperature and requires more time for the completion of the reaction. At higher temperature improved yields of the products are obtained. The reaction could not proceed in the absence of catalyst (Table 2, entry 6), which proves the catalytic role of MNZ-1 in this reaction. Pure ZrO_2 nanocrystals were also found to be completely inactive, whereas pure NiO nanoparticles (BET surface area of $24\text{ m}^2\text{ g}^{-1}$ and devoid of mesoscopic void space, synthesized under similar conditions in the absence of ZrO_2) showed a very poor cross-coupling product (Table 2, entry 7). This result suggests that the surface area and the mesoporosity of our MNZ-1 plays a crucial role in this catalytic reaction. To understand the active species involved in this reaction, we have also used a physical mixture of pure NiO and ZrO_2 in 1 : 1

proportion as catalyst. This physical mixture is also quite less efficient in this C–S coupling reaction (Table 2, entry 8, 36.4% yield). Synergic effects between both species could be responsible for little increase in product yield *vis-à-vis* NiO alone. Since, the reaction proceeds in aqueous medium and under aerobic conditions over our self-assembled mixed oxide nanocatalyst, the method described herein provides a green protocol towards the synthesis of diaryl sulfides.

A probable reaction mechanism for the C–S coupling reaction has been suggested in Scheme 2.³⁴ We have taken FT IR spectra of the catalyst during the catalytic reactions. As soon as the catalyst is added to the reaction medium a red colored complex has been formed between 4-chlorothiophenol and the Ni atom of the catalyst (I) which is proved from the disappearance of the stretching frequency of the S–H bond of the 4-chlorothiophenol in the thio-Ni complex near 2550–2600 cm⁻¹ (Fig. 9).³⁵ The red complex does not react with iodobenzene in the absence of base B here K₂CO₃. Thus K₂CO₃ plays a pivotal role in this reaction and it is proposed that a six membered ring (II) forms during oxidative addition of iodo compound to the catalyst–thiol complex. The other oxide ZrO₂ helps to increase the effective surface area of the catalyst bed and stabilize the active tiny NiO nanocrystals at its surface so that the reaction can proceed more efficiently. Further, inactivity of pure ZrO₂ in this reaction suggests the complex formation of thiol only occurs at the Ni-sites and not on Zr-sites. Electron donating substituent facilitates the coordination of the metal to π -bond of the aromatic ring providing higher conversion. Finally intermediate (II) on reductive elimination *via* species (III) gives the desired product with regeneration of the catalyst during the catalytic reaction process.

Recovery and recycling of the catalyst

After completion of the reaction between 4-iodoanisole and 4-chlorothiophenol in the presence of MNZ-1, the solid catalyst has been filtered off the reaction mixture, washed with water and acetone. Finally it was dried and activated by heating at 673 K in air. The catalyst was then ready for further use for another C–S coupling reaction. Yield of the diaryl sulfide decreased marginally from 89.0 to 87.2% in the second cycle. The wide angle powder XRD data of this sample (Fig. 2c) shows the same pattern as that of the fresh sample. After reusing, the Ni content of MNZ-1 was discovered from AAS analysis. It is observed that 8.5% Ni is present compared to 9.1% as observed before the catalytic reaction. Minor loss in Ni-content is within the range of experimental error.

Conclusions

Self-assembled NiO–ZrO₂ nanocatalyst has been synthesized *via* evaporation induced self-assembly method, which shows mesoscopic assembly of *ca.* 7 nm size nanoparticles. The calcined material is highly crystalline with a cubic crystal structure. This nanocatalyst exhibits good catalytic activity in the C–S cross-coupling reaction in aqueous medium under aerobic conditions using commercially available base K₂CO₃, together with ease of product isolation and recovery. Various diaryl sulfides are formed over this NiO–ZrO₂ nanocatalyst in excellent yields. The

green catalyst developed herein is highly stable and provides a convenient route, which could play an imperative role in the synthesis of numerous target sulfur containing compounds in organic synthesis.

Acknowledgements

AB wishes to thank Department of Science and Technology (DST), New Delhi for financial support. NP is thankful to Council of Scientific and Industrial Research (CSIR), New Delhi for the senior research fellowship.

References

- (a) A. M. Kalsin, M. Paszewski, S. K. Smoukov, K. J. M. Bishop and B. A. Grzybowski, *Science*, 2006, **312**, 420; (b) J. Zhang, S. Ohara, M. Umetsu, T. Naka, Y. Hatakeyama and T. Adschiri, *Adv. Mater.*, 2007, **19**, 203; (c) Y. X. Zhang and H. C. Zeng, *J. Phys. Chem. C*, 2007, **111**, 6970.
- R. P. Andres, J. D. Biefeld, J. I. Henderson, D. B. Janes, V. R. Kolagunta, C. P. Kubiak, W. J. Mahoney and R. G. Osifchin, *Science*, 1996, **273**, 1690.
- A. K. Boal, F. Ilhan, J. E. DeRouchey, T. Thurn-Albrecht, T. P. Russell and V. M. Rotello, *Nature*, 2000, **404**, 746.
- J. Liu, S. Mendoza, E. Roman, M. J. Lynn, R. Xu and A. E. Kaifer, *J. Am. Chem. Soc.*, 1999, **121**, 4304.
- (a) A. N. Shipway, E. Katz and I. Willner, *ChemPhysChem*, 2000, **1**, 18; (b) M. Zhou, S. Chen and S. Zhao, *J. Phys. Chem. B*, 2006, **110**, 4510; (c) H.-B. Xia, J. Yi, P.-S. Foo and B. Liu, *Chem. Mater.*, 2007, **19**, 4087; (d) O. Taratula, A. M. Chen, J. Zhang, J. Chaudry, L. Nagahara, I. Banerjee and H. He, *J. Phys. Chem. C*, 2007, **111**, 7666; (e) S. K. Das, M. K. Bhunia and A. Bhaumik, *Dalton Trans.*, 2010, **39**, 4382.
- P. V. Kamat, *J. Phys. Chem. C*, 2007, **111**, 2834.
- (a) S. Ajaikumar and A. Pandurangan, *Appl. Catal., A*, 2009, **357**, 184; (b) H. Chen, J. Gu, J. Shi, Z. Liu, J. Gao, M. Ruan and D. Yan, *Adv. Mater.*, 2005, **17**, 2010.
- F. Bosco, A. Ayril, P.-A. Albouy, L. Datas and C. Guizard, *Chem. Mater.*, 2004, **16**, 2208.
- V. Polshettiwar and R. S. Varma, *Green Chem.*, 2010, **12**, 743–754.
- (a) H. Cölfen and M. Antonietti, *Angew. Chem., Int. Ed.*, 2005, **44**, 5576; (b) F. Raimondi, G. G. Scherer, R. Kötz and A. Woraun, *Angew. Chem., Int. Ed.*, 2005, **44**, 2190.
- (a) M. Zhang, G. Sheng, J. Fu, T. An, X. Wang and X. Hu, *Mater. Lett.*, 2005, **59**, 3641; (b) G. K. Pradhan and K. M. Parida, *Int. J. Eng. Sci. Technol.*, 2010, **2**, 53.
- (a) A. Bibby and L. Mercier, *Green Chem.*, 2003, **5**, 15; (b) H. Yoshitake, T. Yokoi and T. Tatsumi, *Chem. Mater.*, 2003, **15**, 1713; (c) M. Fujiwara, S. Terashima, Y. Endo, K. Shiokawa and H. Ohue, *Chem. Commun.*, 2006, 4635; (d) G. Sun, Y. Chang, S. Li, Q. Li, R. Xu, J. Gu and E. Wang, *Dalton Trans.*, 2009, 4481; (e) S. L. Jain, B. S. Rana, B. Singh, A. K. Sinha, A. Bhaumik, M. Nandi and B. Sain, *Green Chem.*, 2010, **12**, 374.
- J.-Y. Chane-Ching, F. Cobo, D. Aubert, H. G. Harvey, M. Airiau and A. Corma, *Chem.–Eur. J.*, 2005, **11**, 979.
- H. Chen, J. Gu, J. Shi, Z. Liu, J. Gao, M. Ruan and D. Yan, *Adv. Mater.*, 2005, **17**, 2010.
- J. Ba, J. Polleux, M. Antonietti and M. Niederberger, *Adv. Mater.*, 2005, **17**, 2509.
- D. Grosso, C. Boissière, B. Smarsly, T. Brezesinski, N. Pinna, P. A. Albouy, H. Amenitsch, M. Antonietti and C. Sanchez, *Nat. Mater.*, 2004, **3**, 787.
- M. S. Wong, E. S. Jeng and J. Y. Ying, *Nano Lett.*, 2001, **1**, 637.
- M. B. Gawande, P. S. Branco, K. Parghi, J. J. Shrikhande, R. K. Pandey, C. A. A. Ghumman, N. Bundaleski, O. M. N. D. Teodorod and R. V. Jayaram, *Catal. Sci. Technol.*, 2011, **1**, 1653.
- (a) D. N. Jones, in *Comprehensive Organic Chemistry*, ed. D. H. Barton and D. W. Ollis, Pergamon, New York, 1979, vol. 3; (b) H. J. Cristau, B. Chabaud, A. Chene and H. Christol, *Synthesis*, 1981, 892; (c) W. Y. Wu, J. C. Wang and F. Y. Tsai, *Green Chem.*, 2009, **11**, 326; (d) S. Ranjit, Z. Y. Duan, P. F. Zhang and X. G. Liu, *Org. Lett.*, 2010, **12**, 4134; (e) S. W. Cheng, M. C. Tseng, K. H. Lii, C. R. Lee and

- S. G. Shyu, *Chem. Commun.*, 2011, **47**, 5599; (f) S. Mallick, S. Rana and K. M. Parida, *Dalton Trans.*, 2011, **40**, 9169; (g) I. P. Beletskaya and V. P. Ananikov, *Chem. Rev.*, 2011, **111**, 1596.
- 20 (a) J. Hassan, M. Sevignon, C. Gozzi, E. Schulz and M. Lemaire, *Chem. Rev.*, 2002, **102**, 1359; (b) C. Mispelaere-Canivet, J.-F. Spindler, S. Perrio and P. Beslin, *Tetrahedron*, 2005, **61**, 5253; (c) Y.-C. Wong, T. T. Jayanth and C.-H. Cheng, *Org. Lett.*, 2006, **8**, 5613; (d) L. Rout, T. K. Sen and T. Punniyamurthy, *Angew. Chem., Int. Ed.*, 2007, **37**, 2046.
- 21 J. Mondal, A. Modak, A. Dutta and A. Bhaumik, *Dalton Trans.*, 2011, **40**, 5228.
- 22 B. C. Ranu, A. Saha and R. Jana, *Adv. Synth. Catal.*, 2007, **349**, 2690.
- 23 (a) J. Langer, R. Fischer, H. Görls and D. Walther, *J. Organomet. Chem.*, 2004, **689**, 2952; (b) M. J. Iglesias, A. Prieto and M. C. Nicasio, *Adv. Synth. Catal.*, 2010, **352**, 1949.
- 24 Q. Yuan, A.-X. Yin, C. Luo, L.-D. Sun, Y.-W. Zhang, W.-T. Duan, H.-C. Liu and C.-H. Yan, *J. Am. Chem. Soc.*, 2008, **130**, 3465.
- 25 S. K. Das, M. K. Bhunia, A. K. Sinha and A. Bhaumik, *J. Phys. Chem. C*, 2009, **113**, 8918.
- 26 H. Qiao, Z. Wei, H. Yang, L. Zhu and X. Yan, *J. Nanomater.*, 2009, 795928–795925.
- 27 (a) C. T. Kresge, M. E. Leonowicz, W. J. Roth, J. C. Vartuli and J. S. Beck, *Nature*, 1992, **359**, 710; (b) H. Peng, J. Tang, L. Yang, J. Pang, H. S. Ashbaugh, C. J. Brinker, Z. Yang and Y. Lu, *J. Am. Chem. Soc.*, 2006, **128**, 5304; (c) A. Modak, J. Mondal, M. Sasidharan and A. Bhaumik, *Green Chem.*, 2011, **13**, 1317–1341.
- 28 P. Yang, D. Zhao, D. L. Margolese, B. F. Chmelka and G. D. Stucky, *Nature*, 1998, **396**, 152.
- 29 P. I. Ravikovitch and A. V. Neimark, *Langmuir*, 2002, **18**, 1550.
- 30 G. Stefanic, M. Didovic and S. Music, *J. Mol. Struct.*, 2007, **834–836**, 435.
- 31 G. Katz, *J. Am. Ceram. Soc.*, 1971, **54**, 531.
- 32 D. Srinivas, C. V. V. Satyanarayana, H. S. Potdar and P. Ratnasamy, *Appl. Catal., A*, 2003, **246**, 323.
- 33 ¹H and ¹³C NMR chemical shifts for different diaryl sulfides reported in Table 2 (for spectra see ESI†). **Entry 1**: ¹H NMR (300 MHz, CDCl₃) δ = 6.96–7.01 (1H, t), 7.15–7.30 (7H, m), 7.57–7.60 (1H, d). ¹³C NMR (300 MHz, CDCl₃) δ = 127.5, 129.5, 130.3, 133.7, 135.2. **Entry 2**: ¹H NMR (300 MHz, CDCl₃) δ = 3.62 (3H, s), 6.53–6.54 (2H, d), 7.12–7.13 (2H, d), 7.25–7.26 (2H, d), 7.40–7.42 (2H, d). ¹³C NMR (300 MHz, CDCl₃) δ = 55.3, 116.4, 129.3, 133.6, 135.2, 138.2, 159.4. **Entry 3**: ¹H NMR (300 MHz, CDCl₃) δ = 2.30 (3H, s), 6.91–6.93 (2H, d), 7.26–7.30 (2H, d), 7.40–7.43 (2H, d), 7.55–7.57 (2H, d). ¹³C NMR (300 MHz, CDCl₃) δ = 21.2, 129.7, 131.3, 133.7, 135.2, 137.3, 137.5.
- 34 S. Bhadra, B. Sreedhar and B. C. Ranu, *Adv. Synth. Catal.*, 2009, **351**, 2369.
- 35 D. W. Scott and J. P. McCullough, *J. Am. Chem. Soc.*, 1958, **80**, 3554.